CHEMISTRY OF MATERIALS

COMMUNICATION

pubs.acs.org/cm

Resistance Switching in Electrodeposited VO_2 Thin Films

Jakub A. Koza, Zhen He, Andrew S. Miller, and Jay A. Switzer*

Department of Chemistry and Graduate Center for Materials Research, Missouri University of Science and Technology, Rolla, Missouri 65409-1170, United States

Supporting Information

KEYWORDS: vanadium dioxide, metal-to-insulator transition, resistance switching, electrodeposition

Vanadium dioxide (VO_2) is a compound that undergoes a sharp, first order metal-to-insulator transition (MIT) at a temperature of ~68 °C[1] accompanied by a structural change from an insulating, low-temperature monoclinic form VO_2(M) to a high-temperature, metallic rutile structure VO_2(R).[2−4] The MIT near room temperature (RT) and the ultrafast (~fs) phase transition[5] make this compound a promising candidate for novel electronic applications, such as ultrafast switches, Mott field effect transistors (MottFET), memristors, and solid-state memory.[4,6,7] Since the early discovery of the MIT in VO_2 by Morin in 1959[1] there has been a lot of effort to reveal the MIT mechanism, and to develop and optimize methods for deposition of VO_2 thin films and nanostructures.[4] To the best of the authors' knowledge, only one paper has been published on the preparation of VO_2 by electrodeposition.[8] However, this method can only produce VO_2 layers a few nanometers thick and the as-deposited xerogel has to be stored for 45 days prior to annealing in vacuum. Here, we report that ~140 nm thick VO_2 films can be produced by electrochemical reduction of V^{5+} ions complexed with triethanolamine (TEA), followed by an immediate, short anneal at 400 °C. The films were deposited at 80 °C from a solution of 0.4 M V(V) and 0.25 M TEA at a pH of 6.5.

The electrochemistry of the V^{5+}-TEA was studied by linear sweep voltammetry (LSV) and potentiostatic depositions at 80 °C. Figure 1a shows the LSV at a Pt working electrode (WE), together with corresponding mass changes measured with an electrochemical quartz crystal microbalance (EQCM). Three characteristic potential ranges can be observed (black curve − marked by arrows). Peak I is assigned to be the V^{5+}/V^{4+} redox couple (eq 1). At this potential range the film starts to deposit, i.e. the mass begins to increase (Figure 1a − red curve), according to the proposed mechanism (eqs 1 and 2). Shoulder II corresponds to proton reduction (eq 3) and the steep increase in the curve slope marked as III is the water decomposition (eq 4).

$$V^{5+}(TEA) + e^- \rightarrow V^{4+} + TEA \quad (1)$$

$$V^{4+} + 4OH^- \rightarrow VO_2 \cdot nH_2O + (2-n)H_2O \quad (2)$$

$$H^+ + e^- \rightarrow \frac{1}{2}H_2\uparrow \quad (3)$$

$$H_2O + e^- \rightarrow \frac{1}{2}H_2\uparrow + OH^- \quad (4)$$

In Figure 1b, steady state deposition rates obtained at different potentials calculated by differentiation of the mass vs time transients together with corresponding steady state current densities are shown. It is apparent that as the potential becomes more negative, the deposition rate increases. At potentials more negative than about −0.6 $V_{Ag/AgCl}$, i.e., the onset of the protonic hydrogen reduction (II in Figure 1a), hydrogen evolution occurs (eq 3). This is accompanied by a change of the slope in the deposition rate vs potential dependence. The threshold potential determined from the steady state deposition rate vs potential dependence (Figure 1b) of about −0.65 $V_{Ag/AgCl}$ is very close to the onset potential of protonic hydrogen reduction determined by LSV (−0.6 $V_{Ag/AgCl}$). This is also accompanied by an increase in the steady-state current density due to the proton reduction (Figure 1b).

An increased deposition rate at potentials more negative than the onset of proton reduction is consistent with the proposed mechanism (eqs 1 and 2). The pH of the electrolyte is weakly acidic (pH 6.5). The hydrogen evolution at the WE causes a local interfacial pH increase, that for nonbuffered electrolytes can be significant.[9,10] A higher interface OH^- concentration shifts the reaction 2 equilibrium to the right, and as a result, higher deposition rates are achieved. At potentials more negative than about −0.9 $V_{Ag/AgCl}$ water decomposition sets in. A very strong bubbling at the electrode surface is observed and the current efficiency decays. For potentials more positive than the onset of hydrogen evolution, deposition rates are very low and do not allow the deposition of thick films. Based on these results, a potential of −0.8 $V_{Ag/AgCl}$ was chosen for potentiostatic deposition as a compromise between current efficiency and deposition rate.

A 150 nm thick film was deposited having a light-blue appearance (see the Supporting Information, Figure 1S), and its chemistry was probed by X-ray photoelectron spectroscopy (XPS). High-resolution XPS (HR-XPS) core-level spectra of $V2p_{3/2}$ and O1s for an as-deposited film are shown in Figure 2a,b. The $V2p_{3/2}$ spectrum (Figure 2a) displays a single, symmetric peak with a maximum at 516.3 eV that can be attributed to a single, 4+ oxidation state of vanadium.[11] The O1s spectrum (Figure 2b) can be decomposed into two constituents, i.e., V−O at 530.3 eV and V−OH at 531.4 eV.[12] This indicates that the

Received: July 7, 2011
Revised: August 10, 2011
Published: August 30, 2011

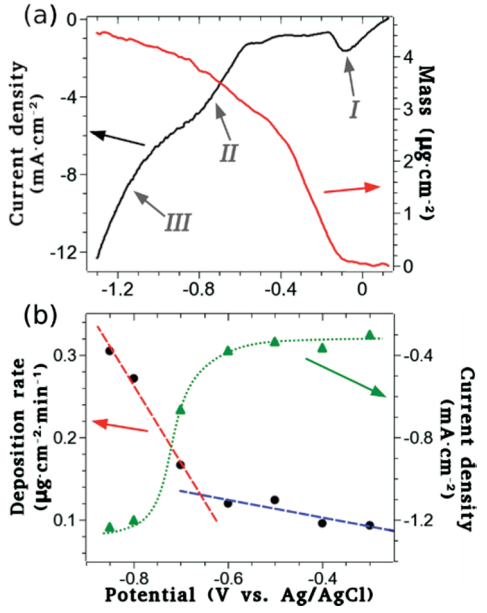

Figure 1. Electrochemistry of V^{5+}-TEA electrolyte at 80 °C on Pt-coated quartz. (a) Linear sweep voltammogram together with corresponding mass changes showing characteristic potential ranges measured at a scan rate of 10 mV s^{-1}. (b) Steady-state deposition rate dependence on the applied potential obtained from mass vs time transients (black circles and dashed lines) and steady state current density vs potential dependence (green triangles and dotted line).

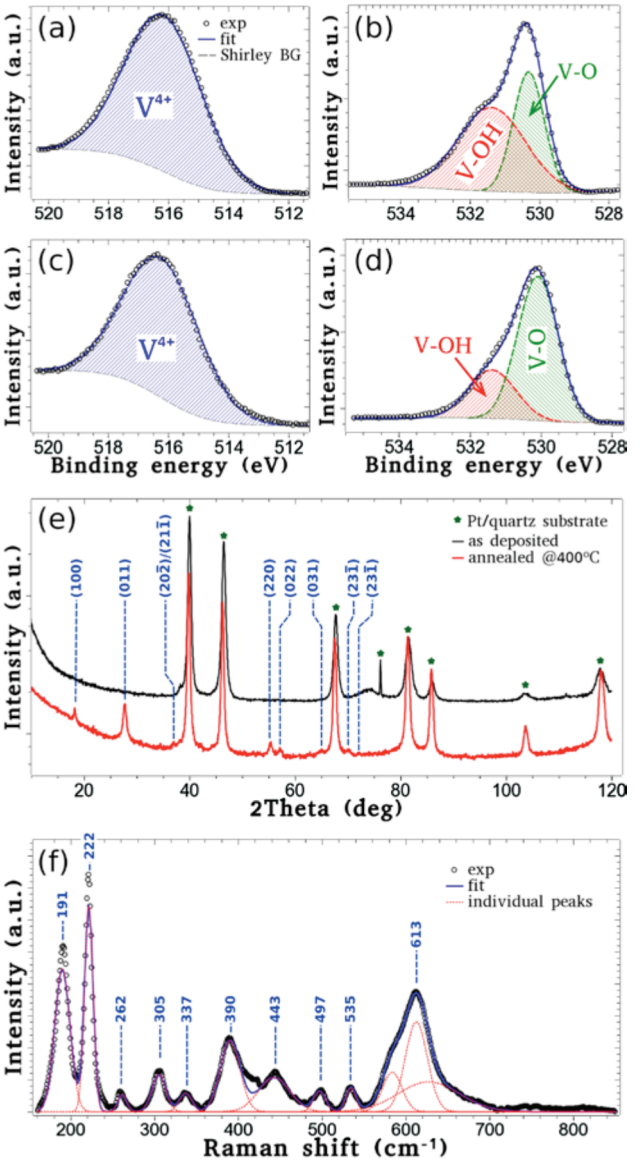

Figure 2. Chemical and structural analysis of as-deposited and annealed film. (a–d) HRXPS spectra (black open points) for (a, b) as-deposited and (c, d) annealed films together with deconvolution of (a, c) V $2p_{3/2}$ and (b, d) O 1s peaks. The fitting of peaks was performed after Shirley background subtraction (gray dashed line) and binding energy correction for specimen charging by referencing the C1s peak position to 284.6 eV. (e) X-ray grazing incident diffraction patterns of the as-deposited (black) and the annealed (red) film. The pattern obtained for the annealed film matches the low-temperature monoclinic form of VO_2 (planes indexed in blue). Substrate peaks are marked with green asterisks. (f) Raman spectrum of the annealed film (black open points) together with multiple-Gaussian peaks fit (blue line) and individual peaks (red dotted lines) characteristic for low-temperature monoclinic VO_2.

as-deposited film is hydrated. Similar results were previously reported for V_2O_5 electrodeposition.[13,14]

To probe the crystallinity of the film, X-ray diffraction (XRD) was performed. In the XRD pattern for the as-deposited film, no peaks originating from the deposit are observed. Only the Pt/quartz substrate peaks are present (black curve in Figure 2e), revealing the amorphous nature of the layer. The amorphous nature of the film was also confirmed by Raman studies (see the Supporting Information, Figure 2S).

The film was annealed at 400 °C in an Ar atmosphere for 1.5 h to dehydrate and crystallize it. After annealing, the film has a thickness of about 140 nm and deep blue appearance (see the Supporting Information, Figure 1S). The SEM and AFM studies have shown that the annealed film is nanocrystalline and dense, with an average grain size of 66 ± 7 nm and roughness (Rms) of 10 ± 1 nm (see the Supporting Information Figure 3S). The HR-XPS spectrum for the annealed film does not show any changes in the vanadium oxidation state (Figure 2c). The O1s spectrum can also be decomposed into two constituents, i.e., V−O and V−OH, however, the V−OH peak area is significantly reduced after annealing. The XRD pattern clearly indicates that the annealing procedure crystallized the film because peaks originating from the deposited layer appeared (red curve in Figure 2e). The XRD pattern obtained for the annealed film fits to VO_2(M). This is further supported by Raman spectroscopy. The Raman spectrum shown in Figure 2f fits to that of VO_2(M).[2,15−18] Lack of a peak at a Raman shift of about 705 cm^{-1}, which is characteristic for V_2O_5,[2,15] confirms the high purity of the annealed layer.

The resistance dependence on temperature ($R(T)$) is shown in Figure 3a. The annealed film undergoes the MIT and also shows characteristic hysteretic behavior.[1,4,7,17,19−21] The determined transition temperatures, 322 K on heating and 306 K on cooling (Figure 3b), are lower than those measured for stoichiometric VO_2 single crystals (341 K).[1] The reason for this is most probably nonstoichiometry in the film that has been shown to have a strong influence on the MIT temperature.[22] However, many other parameters can influence the MIT temperature. For instance, the degree of structural ordering was shown to affect the MIT temperature, as disordered VO_2 films exhibit the transition at much lower temperatures.[23,24] The MIT transition shown in

dx.doi.org/10.1021/cm2019394 |Chem. Mater. 2011, 23, 4105–4108

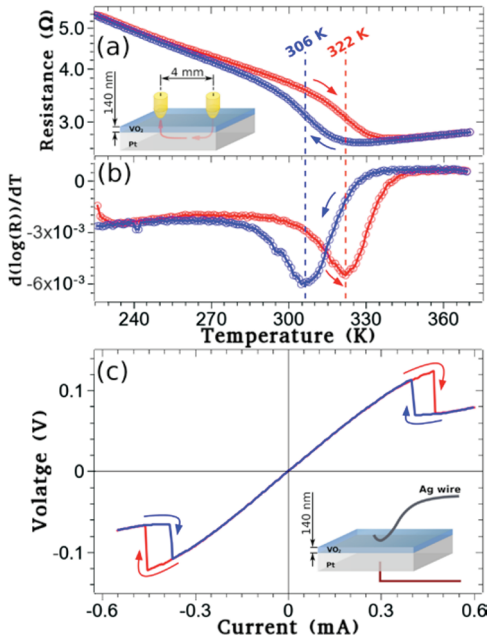

Figure 3. Electrical transport characterization of the annealed VO_2 film. (a) Temperature dependence of the normal to the film plane resistance showing the MIT temperatures upon heating (red) and cooling (blue) measured at 0.5 K min^{-1}. Transition temperatures were determined from (b) a plot of $d(\log(R))/dt$ vs T. (c) $I-V$ characteristic of the VO_2 film measured at room temperature showing reversible resistance switching between the low-temperature monoclinic (insulating) and high-temperature rutile (metallic) phases. The $I-V$ curve was measured by scanning the current at a rate of 0.1 mA s^{-1}.

Figure 3a is broad and the hysteresis is quite wide ($\Delta T = 16$ K). It was demonstrated by other workers that VO_2 has a multidomain structure, even for quasi-1D single-crystalline nanostructures, and insulating or metallic domains can be stable above or below the MIT temperature, respectively, broadening the $R(T)$ hysteresis.[2,18,19,25] Nevertheless, there is a clear MIT for the annealed film and no other transitions at low temperatures were detected (see the Supporting Information, Figure 4S) that could originate from lower vanadium oxides,[1] proving the high purity of the film.

The VO_2 films exhibit resistance switching at room temperature. The $I-V$ dependence for the annealed VO_2 film measured at room temperature is shown in Figure 3c. From Figure 3c, it is apparent that as the current increases, the film shows a switch (negative differential resistance – *NDR*) and on the reverse scan it switches back again. Both the current (~0.5 mA) and voltage (~0.12 V) required to switch the films are quite low. Joule heating of the film probably causes this behavior. At the switching current, the temperature reaches the MIT temperature, leading to an abrupt drop in the resistance. In the backward scan, the opposite direction switch is observed, however at lower current and voltage. This is in agreement with the $R(T)$ dependence, i.e., different MIT temperatures measured upon heating and cooling (Figure 3a,b). However, it has been shown that the MIT could be electric field driven, i.e., Mott-like characteristic,[4,6,26] and this mechanism cannot be excluded.

We have shown that ~140 nm thick VO_2 films can be obtained by electrochemical reduction of V(V), followed by a short thermal treatment at 400 °C. The electrodeposited VO_2 undergoes reversible resistance switching at room temperature with very low power requirements. Possible applications of the material include the fabrication of ultrafast (~fs) switches, memristors, neural networks, and solid-state memory. The electrochemical approach for preparing thin VO_2 films is of interest because it introduces an easy and inexpensive method for depositing onto complex geometry substrates. In contrast with chemical and physical vapor deposition methods, electrodeposition requires a conducting substrate. Although this can be a disadvantage for measuring the electrical properties of the films because of the influence of the substrate, it can be an advantage for device fabrication because the film selectively deposits on an electrically poised conductor. Because electrodeposition is already used to fill up Si trenches with Cu,[27] VO_2 could be electrodeposited directly onto Cu that could act as one of the contacts, omitting one of the lithographic steps necessary for physical deposition methods. Also, because electrodeposition is not a line-of-sight deposition method, it should also be possible to selectively deposit conformal films of VO_2 on the conducting elements of nanocrossbar arrays for solid-state memory.

■ ASSOCIATED CONTENT

Supporting Information. Experimental details; optical, SEM, and AFM images of films; Raman spectrum of the as-deposited film. This material is available free of charge via the Internet at http://pubs.acs.org.

■ AUTHOR INFORMATION

Corresponding Author
*E-mail: jswitzer@mst.edu.

■ ACKNOWLEDGMENT

Research supported by the U.S. Department of Energy, Office of Basic Energy Sciences, Division of Materials Sciences and Engineering, under Award DE-FG02-08ER46518 (electrodeposition, chemical, and structural characterization studies), and the National Science Foundation under Award DMR-1104801 (electrical transport and resistance switching studies).

■ REFERENCES

(1) Morin, F. J. *Phys. Rev. Lett.* **1959**, *3*, 34–36.
(2) Jones, A. C.; Berweger, S.; Wei, J.; Cobden, D.; Raschke, M. B. *Nano Lett.* **2010**, *10*, 1574–1581.
(3) Sohn, J. I.; Joo, H. J.; Ahn, D.; Lee, H. H.; Porter, A. E.; Kim, K.; Kang, D. J.; Welland, M. E. *Nano Lett.* **2009**, *9*, 3392–3397.
(4) Yang, Z.; Ko, C.; Ramanathan, S. *Annu. Rev. Mater. Res.* **2011**, *41*, 337–367.
(5) Baum, P.; Yang, D.-S.; Zewail, A. H. *Science* **2007**, *318*, 788–792.
(6) Hyun-Tak, K.; Byung-Gyu, Ch; Doo-Hyeb, Y; Sung-Lyul, M; Gyungock, K; Kwang-Yong, K.; Yong-Sik, L. *New J. Phys.* **2004**, *6*, 52.
(7) Driscoll, T.; Kim, H. T.; Chae, B. G.; Di Ventra, M.; Basov, D. N. *Appl. Phys. Lett.* **2009**, *95*, 043503.
(8) Cezar, A. B.; Graff, I. L.; Rikers, Y.; Schreiner, W. H.; Mattoso, N. *Electrochem. Solid-State Lett.* **2011**, *14*, D23–D25.
(9) Deligianni, H.; Romankiw, L. T. *IBM J. Res. Dev.* **1993**, *37*, 85–94.
(10) Koza, J. A.; Uhlemann, M.; Gebert, A.; Schultz, L. *J. Electroanal. Chem.* **2008**, *617*, 194–202.
(11) *Handbook of X-ray Photoelectron Spectroscopy*; Chastain, J., Ed.; Perkin-Elmer Corporation: Eden Prairie, MN, 1992.
(12) Silversmit, G.; Depla, D.; Poelman, H.; Marin, G. B.; De Gryse, R. *J. Electron Spectrosc. Relat. Phenom.* **2004**, *135*, 167–175.

(13) Huang, C.-M.; Hu, C.-C.; Chang, K.-H.; Li, J.-M.; Li, Y.-F. *J. Electrochem. Soc.* **2009**, *156*, A667–A671.
(14) Li, J.-M.; Chang, K.-H.; Hu, C.-C. *Electrochim. Acta* **2010**, *55*, 8600–8605.
(15) Piccirillo, C.; Binions, R.; Parkin, I. P. *Chem. Vap. Deposition* **2007**, *13*, 145–151.
(16) Pan, M.; Liu, J.; Zhong, H.; Wang, S.; Li, Z.-F.; Chen, X.; Lu, W. *J. Cryst. Growth* **2004**, *268*, 178–183.
(17) Gurvitch, M.; Luryi, S.; Polyakov, A.; Shabalov, A.; Dudley, M.; Wang, G.; Ge, S.; Yakovlev, V. *J. Appl. Phys.* **2007**, *102*, 033504.
(18) Zhang, S.; Chou, J. Y.; Lauhon, L. J. *Nano Lett.* **2009**, *9*, 4527–4532.
(19) Ramírez, J.-G.; Sharoni, A.; Dubi, Y.; Gómez, M. E.; Schuller, I. K. *Phys. Rev. B* **2009**, *79*, 235110.
(20) Yang, Z.; Ko, C.; Balakrishnan, V.; Gopalakrishnan, G.; Ramanathan, S. *Phys. Rev. B* **2010**, *82*, 205101.
(21) Yang, Z.; Ko, C.; Ramanathan, S. *J. Appl. Phys.* **2010**, *108*, 073708.
(22) Griffiths, C. H.; Eastwood, H. K. *J. Appl. Phys.* **1974**, *45*, 2201–2206.
(23) Chudnovskii, F. A.; Stefanovich, G. B. *J. Solid State Chem.* **1992**, *98*, 137–143.
(24) Stefanovich, G. B.; Pergament, A. L.; Velichko, A. A.; Stefanovich, L. A. *J. Phys.: Condens. Matter* **2004**, *16*, 4013–4024.
(25) Wu, J.; Gu, Q.; Guiton, B. S.; de Leon, N. P.; Ouyang, L.; Park, H. *Nano Lett.* **2006**, *6*, 2313–2317.
(26) Goodenough, J. B. *J. Solid State Chem.* **1971**, *3*, 490–500.
(27) Moffat, T. P.; Wheeler, D.; Huber, W. H.; Josell, D. *Electrochem. Solid-State Lett.* **2001**, *4*, C26–C29.